Alexandria Engineering Journal (2022) 61, 1701–1713

HOSTED BY

Alexandria University

Alexandria Engineering Journal

www.elsevier.com/locate/aej
www.sciencedirect.com

Improved topology of three-phase series resonant DC-DC boost converter with variable frequency control

Mohamed Salem [a,*], Awang Jusoh [b], Mohamed Dahidah [c], Dahaman Ishak [a], Anna Richelli [d], Ibrahim Alhamroni [e], Mohamad Kamarol [a]

[a] *School of Electrical and Electronic Engineering, Universiti Sains Malaysia (USM), Nibong Tebal, 14300 Penang, Malaysia*
[b] *Department of Electrical Power Engineering, Faculty of Electrical Engineering, Universiti Teknologi Malaysia (UTM), Johor 81310, Malaysia*
[c] *School of Engineering, Newcastle University, Newcastle upon Tyne NE1 7RU, UK*
[d] *Department of Information Engineering, University of Brescia, 25121 Brescia, Italy*
[e] *Department of Electrical, Electronics, University Kuala Lumpur British Malaysian Institute (UniKLBMI), Gombak 53100, Malaysia*

Received 9 April 2021; revised 14 May 2021; accepted 21 June 2021
Available online 03 July 2021

KEYWORDS

DC-DC converter;
Series resonant converter (SRC);
Three-phase;
Zero voltage switching (ZVS);
Variable frequency control

Abstract This paper proposes an improved topology of the three-phase series resonant DC-DC Boost converter with variable frequency control. The DC output voltage can be properly regulated at a constant value from no-load condition to full-load condition by adjusting the switching frequency. This is feasible with the three series resonant circuits coupled to the three-phase inverter. The leakage and mutual inductances of the step-up transformer are used implicitly in the series resonant circuits. Therefore, the proposed converter, when matched to the traditional three-phase inter-leaved LLC converters, requires fewer transformers, passive components, and switching devices. Furthermore, it offers better efficiency and size reduction. The proposed SRC converter also relies on the transformer's magnetizing inductance to ensure zero voltage switching (ZVS) for all the switches within the considered range of the operating frequency. The deployed variable frequency controller shows a good level of stability at the considered loading conditions. The output voltage-to-input voltage ratio is steadily regulated at 6:1, irrespective of the load variation, by varying the switching frequency. The experimental validation of the theoretical findings proceeded on a

* Corresponding author at: School of Electrical and Electronic Engineering, Universiti Sains Malaysia, Engineering Campus, 14300 Nibong Tebal, Pulau Pinang, Malaysia.
E-mail address: salemm@usm.my (M. Salem).

Peer review under responsibility of Faculty of Engineering, Alexandria University.

https://doi.org/10.1016/j.aej.2021.06.078

low power scaled-down laboratory prototype. From the achieved results, the performance of the proposed converter (in terms of its effectiveness) was validated.

1. Introduction

The recent drive for clean energy in power systems, coupled with the increasing industrial applications, such as in smart-grids, electric vehicles, and renewable energy systems, has led to a substantial interest in DC/DC resonant converters. These resonant converters have the advantages of high-frequency operations with soft switching, smooth waveforms, high-power density, and high-efficiency [1–3]. The soft switching merit undoubtedly allows the converter to experience reduced switching losses, even when operating at a high switching frequency [4–6]. The classification of the behavior of resonant converters might depend on many variables, such as their switching technique, frequency ratio, and mode of operation. A converter can achieve ZVS commutation for all switches if it achieves a higher switching frequency than the resonant frequency [7]. Alternatively, a higher resonant frequency than the switching frequency results in zero current switching (ZCS) [8,9]. Series resonant converters (SRC) are popular for many applications due to their simplicity [10,11]. However, their disadvantage is the requirement to split the input voltage between the load and the resonant impedance, which always reduces the DC gain of SRC below unity [12,13]. Furthermore, it is difficult to control the output voltage during no-load or light load conditions. This limits the ZVS to a specific range of input voltage and load conditions [14–16]. To address these issues, several approaches have been considered; one such approach is the *LLC* series resonant converter topology. This has attracted much attention due to its high voltage gain and better conversion efficiency [17,18]. These converters have been developed and investigated for both full-bridge and half-bridge inverter topologies, and with either center-tapped or full-bridge rectifiers at the secondary-sides [19,20]. Utilizing the magnetizing or leakage inductance can further widen the range of the soft switching for all power switches. Hence, high power density and efficiency can be achieved [21,22]. A phase-shifted series resonant converter utilizing stepped-up transformer is implemented in [21]. As a result, the resonant tank inductivity is enhanced, so ZVS is achieved for all single-phase inverter switches. Moreover, the gain is up to a three-fold increase over the input voltage.

Despite the popularity of the single-stage resonant converters, they remain prone to certain drawbacks. This is the case especially when they are used in high input voltage scenarios, where efficiency and reliability are both affected negatively by the current stress on power semi-conductor devices [23,24]. Owing to this limitation, multilevel converters were introduced, as they make the use of low-voltage switching devices possible in high-voltage applications, such as HVDC utility grid applications and medium voltage motor drives [25,26]. Furthermore, the switching frequency range defines the modes of operation of the existing three-phase three-level converters. This has been presented in [27] where the achieved soft switching range is larger compared to that of the PWM-controlled three-phase three-level converter presented by [28]. Soft switching converters are developed for applications that require higher efficiency, smaller size and volume, where high switching frequency can be used with manageable or minimized stress on switching devices [29–31]. Alternatively, the multi-phase parallel technique was proposed in [32] to reduce the current stress in each phase, but the resonant frequency was not the same in each individual *LLC* phase, which may cause imbalanced output currents. Similarly, [33] suggested a three-phase inter-leaved *LLC* resonant converter that is ideal for application in high-voltage scenarios with attainable ZVS. This converter consists of 3 full-bridge LLC resonant converters that are connected to the related secondary component using Y-connected diode rectifiers. The study by [34] exploited the phase-shift technique to hybridize three-phase and *LLC* control. The aim was to reduce the conduction-related losses by splitting the lagging switches among the deployed *LLC* and three-level converters at the primary transformers' side. This also reduces the circulating current, while the secondary sides of three-level and *LLC* converters are connected by an active switch leading to higher converter efficiency.

This paper presents and proposes a new three-phase SRC which, when compared to the traditional three-phase inter-leaved *LLC* converter, provides high output voltage gain with a reduced number of switching devices. With the use of identical *LC* tanks connected in series with a step-up transformer, the proposed converter attains balanced resonant currents and a wide range of ZVS.

2. Proposed converter topology and characteristics

The proposed converter made up of a three-phase inverter, series resonant tanks, step-up transformer, and full-bridge rectifier, as shown in Fig. 1. Although the structure is similar to the conventional hard-switching converters, the utilization of series resonant tanks enables high switching frequency with ZVS operation.

2.1. Circuit configuration of the proposed converter

The resonant tanks of the proposed converter shown in Fig. 1 are identical, i.e., $L_{r1} = L_{r2} = L_{r3}$ and $C_{r1} = C_{r2} = C_{r3}$, to ensure a trade-off between the resonant currents and voltages in the resonant circuits, i.e., $i_{Lr1}, i_{Lr2}, i_{Lr3}, v_{Cr1}, v_{Cr2}$, and v_{Cr3}. The resonant tanks must behave inductively for all the inverter switches ($S_1 - S_6$) to achieve ZVS. The resonant tank inductivity is enhanced by utilizing the transformer leakage inductance. Therefore, the operating region is chosen accordingly to ensure all the switches can achieve the ZVS. It is also expected that each resonant tank should deliver one-third of the required power at the output load. To address the problems of the series resonant [27,35], a three-phase step-up transformer is added to

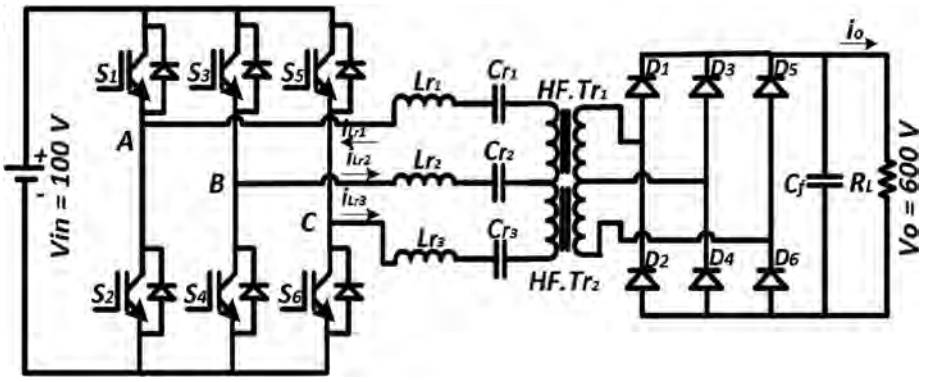

Fig. 1 Schematic depiction of the suggested three-phase series resonant converter.

increase the converter voltage gain and to provide a wider range of ZVS. As depicted in Fig. 1, the transformer's primary windings are linked to the end of the resonant tanks to ensure a balanced current flow through the tanks. Since the secondary windings are linked to the three-phase bridge rectifier, there is a balance in the secondary currents. Varying the switching frequency regulates the output voltage, which makes it possible to vary the load operation with ZVS.

2.2. Circuit characteristics

The following Fourier series can be used to represent the instantaneous three-phase voltages of the voltage source inverter, as depicted in Fig. 1.

$$\mathrm{V_A(t)} = \frac{4\mathrm{V_{in}}}{\pi} \sum_{\mathrm{n=1,3,5,\cdots}} \frac{1}{\mathrm{n}} \sin(\mathrm{n}\omega_\mathrm{s}\mathrm{t}) \tag{1}$$

$$\mathrm{V_B(t)} = \frac{4\mathrm{V_{in}}}{\pi} \sum_{\mathrm{n=1,3,5,\cdots}} \frac{1}{\mathrm{n}} \sin\left(\mathrm{n}\omega_\mathrm{s}\mathrm{t} - \mathrm{n}\frac{2\pi}{3}\right). \tag{2}$$

$$\mathrm{V_c(t)} = \frac{4\mathrm{V_{in}}}{\pi} \sum_{\mathrm{n=1,3,5,\cdots}} \frac{1}{\mathrm{n}} \sin\left(\mathrm{n}\omega_\mathrm{s}\mathrm{t} - \mathrm{n}\frac{4\pi}{3}\right). \tag{3}$$

where ω_s is the angular switching frequency, V_{in} is the dc input voltage and n is the harmonic number. Consequently, the line-to-line voltages V_{AB}, V_{BC} and V_{CA} that are connected to the resonant tanks can be obtained by:

$$V_{AB}(t) = \frac{4V_{in}}{\pi} \sum_{n=1,3,5,\cdots} \frac{1}{n}\left(\sin(n\omega_s t) - \sin n\left(\omega_s t - \frac{2\pi}{3}\right)\right). \tag{4}$$

$$V_{BC}(t) = \frac{4\mathrm{in}}{\pi} \sum_{n=1,3,5,\cdots} \times \frac{1}{n}\left(\sin n\left(\omega_s t - \frac{2\pi}{3}\right) - \sin n\left(\omega_s t - \frac{4\pi}{3}\right)\right). \tag{5}$$

$$V_{CA}(t) = \frac{4V_{in}}{\pi} \sum_{n=1,3,5,\cdots} \times \frac{1}{n}\left(\left(\sin n\left(\omega_s t - \frac{4\pi}{3}\right)\right) - (\sin(n\omega_s t))\right). \tag{6}$$

The AC equivalent circuit depicted in Fig. 2 shows that the resonant tanks' voltage gain can be derived from the ratio of the output impedance to the total input impedance as follows:

$$G = \frac{\frac{\bar{V}_R}{nT}}{\bar{V}_{AB}} = \frac{Z_o}{Z_i} = \frac{\frac{j\omega_s L_m . R_e}{R_e + j\omega_s L_m}}{2j\omega_s L_r - \frac{2j}{\omega_s C_r} + \frac{j\omega_s L_m . R_e}{R_e + j\omega_s L_m}}. \tag{7}$$

where V_R is the output voltage, nT is the transformer winding ratio, Z_o is the output impedance, Z_i is the input impedance, L_r is the transformer leakage inductance, L_m is transformer magnetizing inductance and R_e is the equivalent load resistance referred to the primary side. The following expressions give the resonant circuit parameters:

$$\omega_0 = \frac{1}{\sqrt{L_r C_r}}, A = \frac{L_r}{L_m}. \tag{8}$$

$$Q = \frac{Z_o}{R_e} = \frac{\omega_0 L_r}{R_e} = \frac{1}{\omega_0 C_r R_e}. \tag{9}$$

where ω_0 = the angular resonant frequency, A = ratio of the resonant inductance L_r to the magnetizing inductanceL_m, Q = the load quality factor. The rearrangement of Eq. (7) using Eqs. (8) and (9), coupled with the consideration of the transformer ratio, gives the converters' voltage gain as follows:

$$G = \frac{\frac{2\bar{V}_R}{nT}}{\bar{V}_{AB}} = \frac{Z_o}{Z_i} = \frac{1}{\sqrt{2(1+A)^2\left[1 - \left(\frac{1}{f_N}\right)^2\right]^2 + \left[\frac{1}{Q}\left(f_N \frac{A}{A+1} - \frac{1}{f_N}\right)\right]^2}}. \tag{10}$$

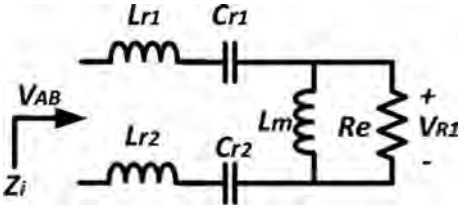

Fig. 2 AC equivalent circuit between two resonant tanks.

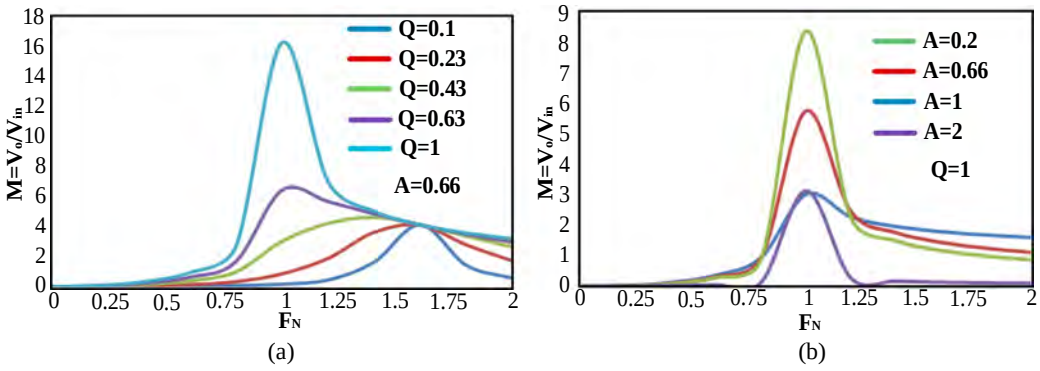

Fig. 3 Voltage gain versus normalized frequency of the proposed three-phase SRC. (a) Different load factors with constant $A = 0.66$. (b) Different inductance ratios with constant$Q = 1$.

where f_N is the normalized frequency, $f_N = f_s/f_0$, f_s is the switching frequency and f_0 is the resonant frequency.

Fig. 3(a) depicts the relationship between the switching frequency and converter gain for different Q values. Evidently, a higher switching frequency than the resonant frequency ($f_N \geq 1$) implies that the converters' output voltage is greater than the input for all the considered switching frequencies($35kHz < f_s < 45kHz$). The gain improves as the switching frequency approaches the resonant frequency, as evidenced for a range of ≥ 0.63, where the achieved output voltage is a sixfold increase over the input voltage. In contrast, at small Qvalues($e.g. Q = 0.1$), the voltage can still be stepped up by the converter but only for a narrow range.

Moreover, the converter gain-switching frequency relationship for different values of inductance ratio A is depicted in Fig. 3(b). It is clear that for A =less than 1, the converter gain can be stepped-up for the whole operating range. On the other hand, when the inductance ratio is larger than 1, the converter can boost the gain. However, this is only for a limited range that is unable to cover whole operating range ($35kHz < f_s < 45kHz$). Thus, for these reasons, and to ensure safe operational modes, the inductance ratio is selected to be less than 1. This means the magnetizing inductance L_m must be larger than the resonant inductanceL_r. It can be seen in Fig. 4, for A values that are less than 1, the converter can achieve the required boost gain (a sixfold increase over the input voltage) for the entire operating range. Meanwhile, for A values that are higher than 1, the voltage gain is much higher than expected at a higher switching frequency; it is closer to the maximum switching frequency ($45kHz$).Being thatSince the devices are selected to achieve 600 V, this might cause damage to the converter equipment. Thus, the proposed converter was considered as the one nearest to the LLC converter. In this case, the equivalent magnetizing inductor can be designed with a large value so the magnetizing current can be reduced, as mentioned in [36,37].The analysis above confirms that the proposed converter is capable of producing higher output voltage than conventional series resonant converters.

Based on the selected design parameters and the input impedance formula presented in Eq. (7), the input impedance angle-switching frequency relationship for a range of effective load resistance values R_e is depicted in Fig. 5. Here, the series resonant tank was observed to provide the inverter with an effective inductive load for all R_e values within the entire operating range ($35 - 45kHz$). This is due to the selection of a large value of L_m, proving that the primary switches have the ability to achieve ZVS. Furthermore, the three-phase voltages of the inverter are phase-shifted by $\pi/3$. This might explain the condition of achieving ZVS for all switches, by ensuring that the input impedance angle Z_i is positive (inductive) for the operating range, as shown in Fig. 5. As a result, the voltage waveform zero-crossed even before the occurrence of the sinusoidal input current waveform, proving the capability of the switches to achieve turn-on at ZVS.

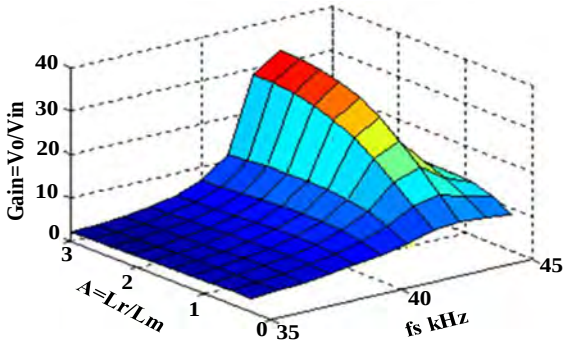

Fig. 4 Voltage gain against various values of $A$and switching frequencies.

3. Principle of operation

The analysis of the proposed SRC and its different operating modes are based on the assumption that all series resonant tanks are identical, i.e., $L_{r1} = L_{r2} = L_{r3}$ and$C_{r1} = C_{r2} = C_{r3}$. In addition, the transformer is also applied with the same turn ratio and magnetizing inductance. This ensures balanced three-phase resonant currents and voltages, as illustrated in Fig. 6. Furthermore, all the switches ($S_1 - S_6$)are allowed a dead time of $0.5us$for to ensure their safe operation. There are seven operating modes for the converter within a half switching cycle. These are described in the following subsections.

3.1. Mode 1 ($t_0 < t < t_1$)

At the start of this mode, switch S_3 is turned off and the applied voltage across is equal toV_{in}, whereas both S_2 and S_5

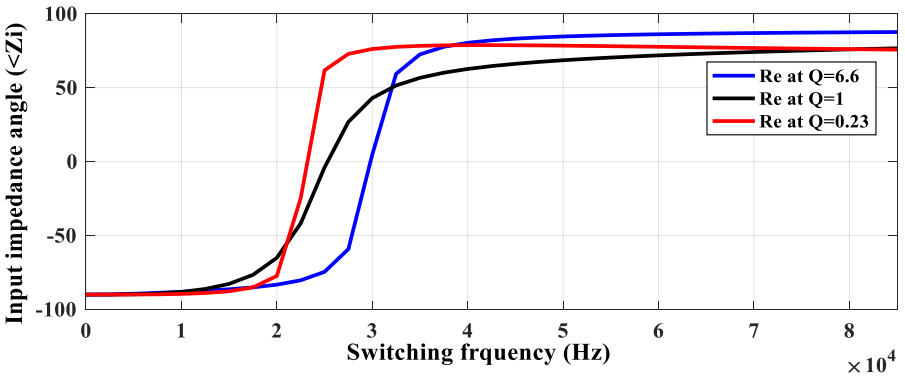

Fig. 5 Relationship between impedance angle and switching frequency at different values of.R_e.

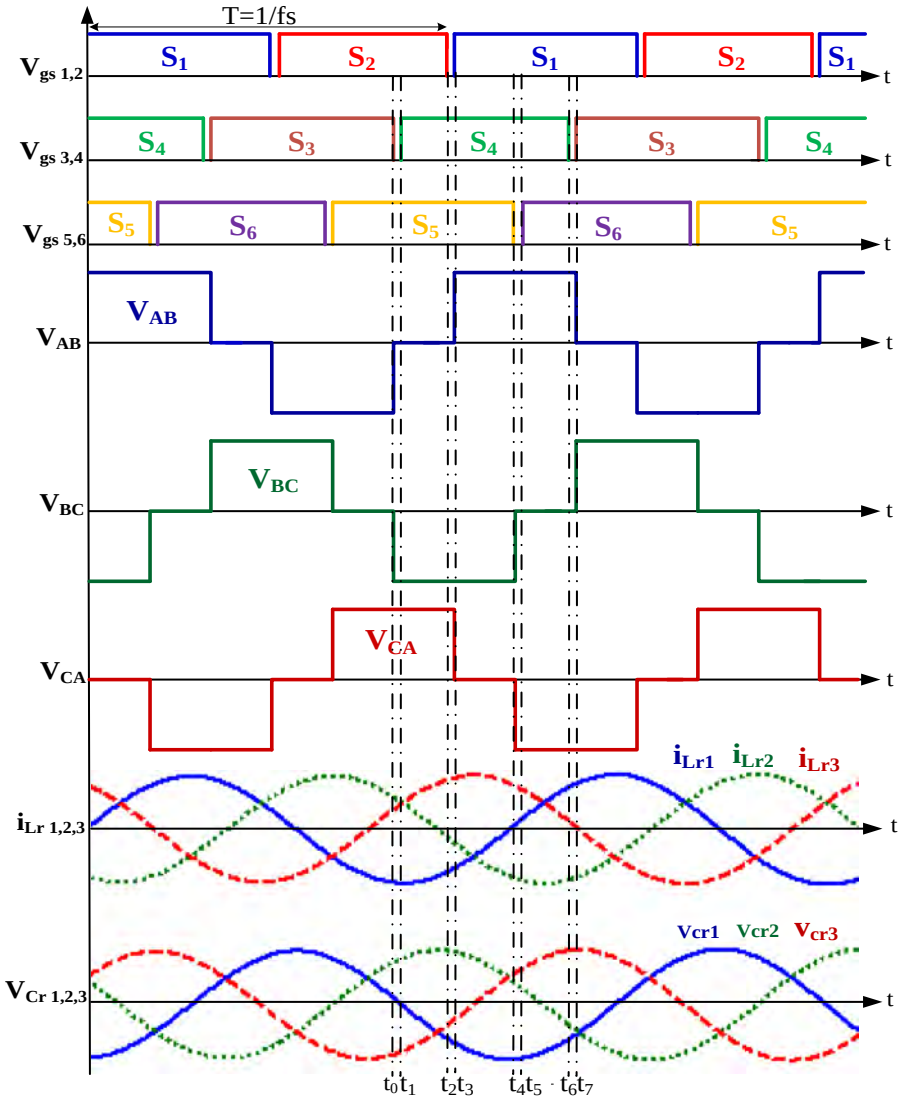

Fig. 6 Theoretical key waveforms of the proposed converter.

are still on. At this instance, V_{AB} drops to zero and V_{CA} is equal toV_{in}, while V_{BC} starts its negative cycle ($-V_{in}$). In this mode, i_{Lr2} starts to decrease and v_{cr2} is charging up. Consequently, the second resonant tank resonates, causing the freewheeling diode of S_4, which is conducted at the end of this mode. The transformer aids in the transfer of the stored energy in the resonant tank to the output load. Fig. 7(a) shows the rectifier diodes (D_2, D_3 and D_6) at the secondary side.

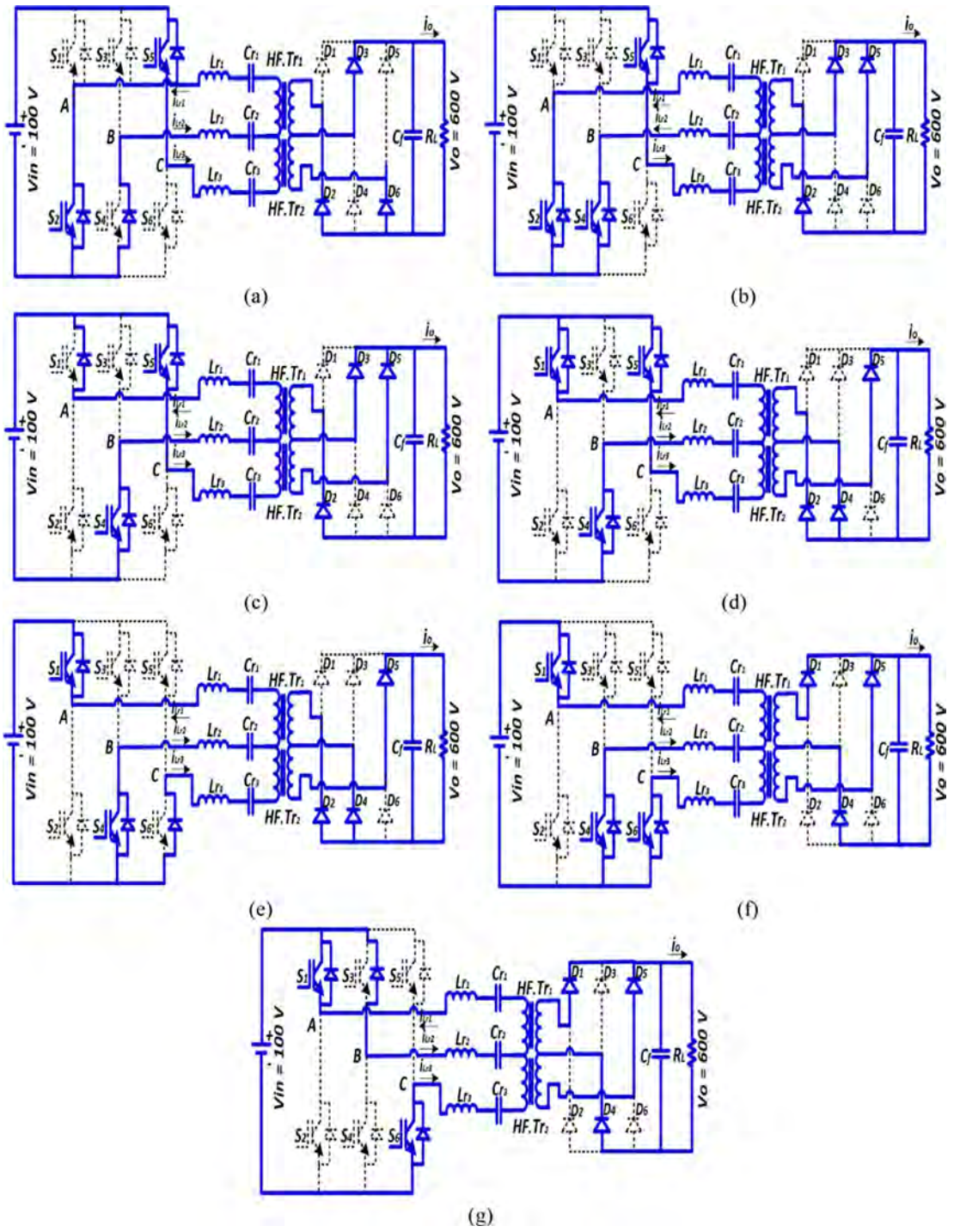

Fig. 7 Operating modes of the proposed converter: (a) Mode 1. (b) Mode 2. (c) Mode 3. (d) Mode 4. (e) Mode 5. (f) Mode 6. (g) Mode 7.

3.2. Mode 2($t_1 < t < t_2$)

As the freewheeling diode of S_4 is conducting at the end of mode 1, it allows S_4 to turn on at ZVS. The resonant capacitor C_{r2} becomes fully charged in this mode. In addition, the stored energy in L_{r2} starts to transfer to the secondary side of the transformer as the rectifier diodesD_2, D_3, and D_5 are conducting, as shown in Fig. 7(b). Consequently, the resonant current i_{Lr2} decreases to zero and starts its negative polarity. It should be noted that both S_2 and S_5 are still on in this mode, causing V_{AB}, V_{BC}, and V_{CA} to retain their previous states as in Mode 1.

3.3. Mode 3 ($t_2 < t < t_3$)

This mode begins when S_2 is turned off, where i_{Lr1} starts to decrease and v_{cr1} builds up, making the first resonant tank start to resonate. As shown in Fig. 7(c), both S_4 and S_5 are on, and the rectifier diodesD_2, D_3, and D_5 are conducting during this

mode. V_{AB} remains at the same state as in the previous mode. However, at the end of this mode, V_{AB} has the same value as V_{in}, and V_{CA} drops to zero. Moreover, to achieve the ZVS, the resonant inductor must reserve more energy than the resonant capacitor, since the end of this mode marks the beginning of the freewheeling diode of S_1.

3.4. Mode 4 ($t_3 < t < t_4$)

The conduction of the freewheeling diode of S_1 at the end of last mode enables S_1 to switch with ZVS at the start of this mode. Tank inductor $L_{r1}$is also discharging and i_{Lr1}reaches zero at the end of this mode. However, the voltage of the resonant capacitor$v_{cr1}$is building up to reach the maximum. This enables the resonant tank to again feed energy to the secondary side. As the rectifier diodesD_2, D_4, and D_5 begin to conduct, the output capacitor filter C_f begins to be recharged. At the end of this mode,V_{AB},V_{BC} and V_{CA} retain the same values of the previous mode, since $S_4$and S_5 remain in the conducting state.

3.5. Mode 5($t_4 < t < t_5$)

At the initial phase of this mode, switch S_5 is turned off and the voltage across it is equal toV_{in}. In this mode, both S_1 and S_4 are on, makingV_{BC} drop to zero. Meanwhile, V_{AB} is equal to $V_{in}$and V_{CA} is equal to$-V_{in}$. On the other hand, i_{Lr3} is decreasing and v_{cr3} is building up during this mode. As shown in Fig. 7(e), the stored energy in L_{r3} and C_{r3} is fed to the output load via D_2, D_4, and D_5. Therefore, the third resonant tank is resonating, causing the conducting of the freewheeling diode ofS_6 at the end of this mode.

3.6. Mode 6 ($t_5 < t < t_6$)

At the beginning of this mode, S_6 turns on with a ZVS due to the conduction of the freewheeling diode of S_6 at the end of the preceding mode. The third tank inductor continues to discharge and its current, i_{Lr3}, starts the negative polarity during this mode. Meanwhile, the resonant capacitor energy is still increasing to reach the maximum value, while the rectifier diodes D_1, D_4, and D_5 are conducted as illustrated in Fig. 5 (f). Once again, S_1 and S_4 maintainsV_{AB}, V_{BC}, and V_{CA} at the same values, just like in the preceding mode.

3.7. Mode 7 ($t_6 < t < t_7$)

Switch S_4 is turned off at the beginning of this mode and i_{Lr2} reaches its highest allowable negative value and ceases to increase. Thus, the voltage across S_4 is proportional to the dc source voltage. The capacitance and inductance of the second tank begins to resonate. S_1 and S_6 are on in this mode and each of V_{AB},V_{BC}, and V_{CA} maintain the same values as the preceding mode; D_1, D_4, and D_5 (rectifier diodes) are all conducting. The conducting of the freewheeling diode of S_3 at the end of this mode repeats the mode 1 operation, where S_3 switches at ZVS, V_{AB} drops to zero, and V_{BC} is equal to V_{in}.

4. Circuit parameters

As illustrated in Fig. 3, the converter voltage gain depends on the switching frequency, f_s and the load quality factor, Q. Therefore, the maximum gain,G_{max}can be achieved by imposing the switching frequency as close as possible to the resonant frequency. The quality factor Q at full-load ($R_L = 330\Omega$) is 0.43. The equivalent turns ratio of the transformer can be calculated by

$$n_{eq} = \frac{V_{in\_min} G_{max}}{2V_o}. \tag{11}$$

So the turns ratio of the transformer is$n_T = \frac{n_{eq}}{2}$. At full load, the minimum load resistance can be calculated by

$$R_{load\_min} = \frac{V_o}{I_{o\_max}}. \tag{12}$$

The effective resistance R_e is the corresponding AC resistance that consists of the rectifier bridge with the capacitor and the load. R_e can be derived as

$$R_e = \frac{16{n_T}^2}{\pi^2} R_{load}. \tag{13}$$

From (9), the calculation of the value of the resonant inductor can be made, thus:

$$L_r = \frac{QR_e}{\omega_0}. \tag{14}$$

Substituting (14) into (8), the resonant capacitor is given by

$$C_r = \frac{1}{L_r \times {\omega^2}_0}. \tag{15}$$

Based on the circuit analysis and the voltage gain in (10), one can obtain the expression that completely describes the proposed converter characteristics. To confirm the selected switching frequency range, the gain has been calculated using the lower and the maximum values of the switching frequency. In order to obtain the desired output voltage of 600 Vdc at a lower switching frequency of $35kHz$, the value of Q must equal

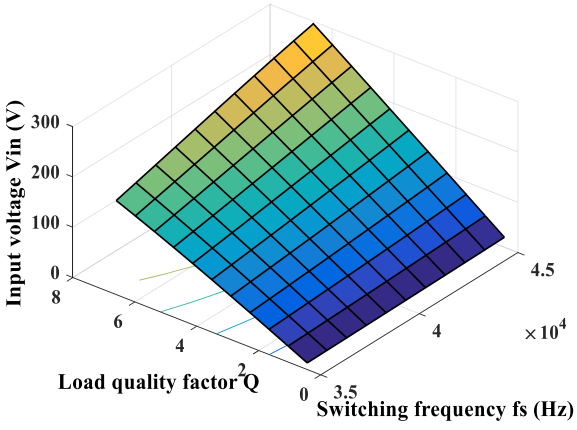

Fig. 8 The input voltage of the proposed SRC at different switching frequencies and load factors.

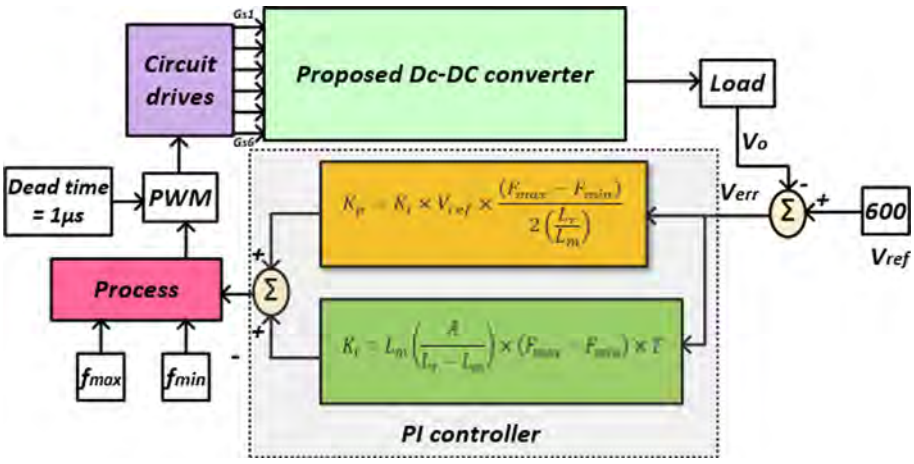

Fig. 9 The block diagram of the variable frequency control.

0.63. However, the same output value can be obtained at the optimal switching frequency of $45kHz$ by varying the load so the value of $Q = 0.43$, as depicted in Fig. 8. It was noticed that changing the input voltage can also meet the variation of the switching frequency while keeping the same load value. Therefore, the desired output voltage can be achieved by the proposed converter by varying the input voltage within the range of $100 - 325$V. To regulate the output voltage of the three-phase converter, the variable frequency control is applied by varying the switching frequency. The maintenance of the output voltage at a specific range demands that the switching frequency be selected following the gain curves exhibited in Fig. 3. The range of the switching frequency must be limited within $35kHz < f_s < 45kHz$ in order to keep the output voltage within $600Vdc$.

The proposed variable frequency control block diagram is shown in Fig. 9. A PI controller with $(K_P = 3000, K_i = 0.002)$ processes the error signal V_{error} between the voltage measured (output voltage) V_o and the voltage required (reference voltage) $V_{ref} = 600V$ is processed by. Thus, all deviations from the output requirements depend on the error sign. Meanwhile, the function of the controller is to raise or lower the switching frequency according to the output voltage required. Next, controlled switch pulses are produced by the controlled switching signal f_s being applied through PWM. In this case, the fixed duty cycle is 50%, while for all switches $(S_1 - S_6)$, a dead time of $0.5\mu s$is consideredwas taken into account to ensure safe operations and that ZVS would be achieved. Consideration was also given to the phase shift between the leg signals.

Table 1 System parameters and specifications of the proposed converter.

Input voltage Vin	100Vdc
Output voltage	$600Vdc$
Switching frequency range	$35 - 45kHz$
Active Switches$(S_1 - S_6)$	$IRGP35B60PDPBF$
Resonant inductances$(L_{r1} = L_{r2} = L_{r3})$	$200\mu H$
Resonant capacintances$(C_{r1} = C_{r2} = C_{r3})$	$70nF$
Magnatizing inductance(L_m)	$300\mu H$
Output capacitance(C_f)	$470\mu H$
Load resistance(R_L)	330Ω
Microcontroller	$TMS320F28335$

5. Experimental results

A scaled-down laboratory prototype was developed to experimentally validate the theoretical findings. Table 1 tabulates the system parameters and specifications, while Fig. 10 shows the experimental set-up. The gate signals of the upper switches of the three-phase inverter are shown in Fig. 11. It is worth noting that the lower switches are complementary to the upper ones, with a sufficient dead time of $0.5\mu s$. Fig. 12 shows the line voltages of the proposed three-phase inverter, which portrays a phase shift of 120^o. Furthermore, the measured waveforms of resonant currents and voltages are depicted in Fig. 13; these clearly show the capability to achieve ZVS for all the switches.

The ZVS was further experimentally validated by measuring the gate and collector-to-emitter voltages for each switch at both light load and full-load conditions, as illustrated in Figs. 14 and 15, respectively. As can be observed, the collector voltage V_{CE} drops to zero for the gate voltage V_{GE} to begin to increase, meaning that all the switches are turned on at ZVS. Furthermore, the system's dynamic response is evaluated by varying the load steps, as depicted in Fig. 16 (load was varied from $0.63kW$ to $1kW$, i.e., 526Ω to 330Ω). From the results, the proposed converter exhibited a good level of response to load step variation while ensuring stability in the output voltage. Notably, there is a small voltage dip during the load change. This required a settling time of$0.02sec$ to maintain the same output voltage. Fig. 17 depicts the calculated output power of the proposed SRC converter at varying operating frequencies with an input voltage of 100Vdc. It was found that the highest power (i.e., $1kW$) was achieved at frequencies much closer to the resonant frequency, while the power decreases as the switching frequency decreases. The efficiency of the converter was also measured, and is shown in Fig. 18.

The proposed converter achieved a maximum efficiency of 94.2% within the considered range of operating frequency. Therefore, it was considered more efficient than the converter discussed in [28]. The breakdown of the loss at full load and at 25% load condition (LC), based on the calculation of the par-

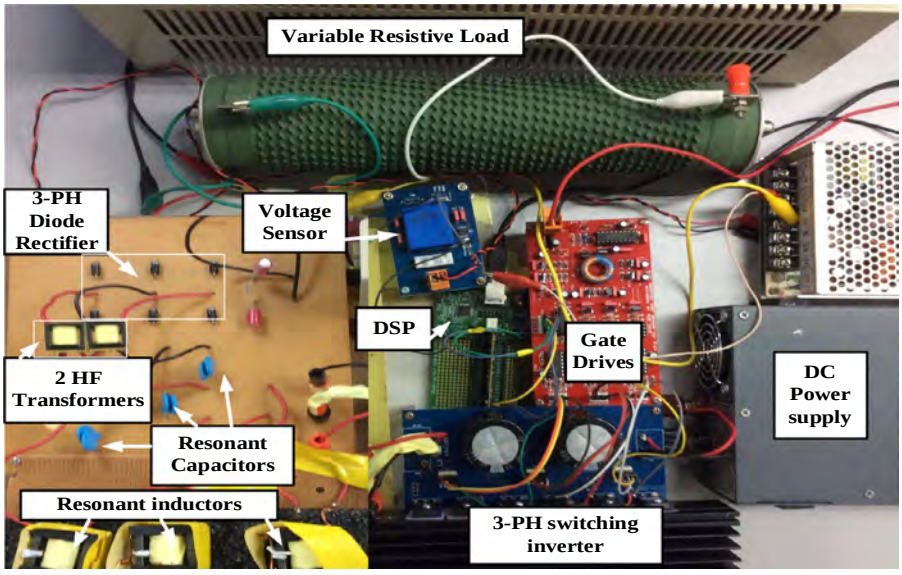

Fig. 10 Experimental set-up of the proposed SRC.

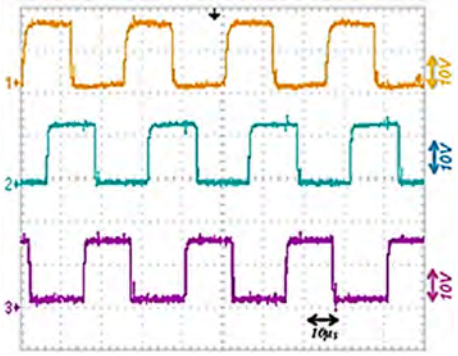

Fig. 11 Measured waveforms of gate signals applied to upper switches: $S1, S3$, and $S5$ respectively.

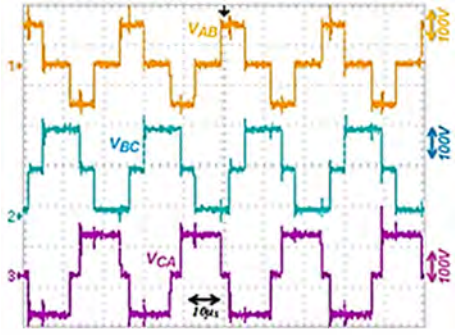

Fig. 12 Measured waveforms of the line voltages.

tial loss of the converters, is presented in Fig. 19. The observed loss breakdown at 25% LC is below that of the full LC, implying that the switching, conduction, and inductor core-related losses decrease significantly at lower loads. This agrees with the results discussed in [38,39]. The reactive power induced the nonlinear reduction of the resonant current towards the output power, causing a notable drop in the efficiency at light load. However, the most prominent losses are the turn-off and the conduction-related switch losses. With the turning-on of the switches at ZVS, there was a significant increase in efficiency. The loss breakdown and the efficiency data support the argument that the proposed converter is suitable for deployment in high voltage applications. Appendix A provides a brief summary of the detailed calculation of loss, as well as the parameters and equations utilized.

The proposed SRC was further evaluated by benchmarking it against alternative three-phase three-level DC/DC converters. It was observed that the projected SRC requires fewer switching devices than the three-phase interleaved LLC proposed in [33]. Moreover, it has the same number of switching devices as the topologies of [27,28]. However, in terms of the number of required transformers, the proposed SRC requires only one transformer, compared to the three transformers needed for the other topologies. It should also be noted that only the projected SRC in this study works as a step-up converter as the other converters only work as voltage step-down, which is a major limitation to their deployment. The analysis also showed that the proposed SRC can work with a wide load variation Q ranging from $Q = 0.23$ to 6.6. This is considered much wider than the topology in [27], which could vary within the range $Q = (1.2 - 6)$. Besides, the proposed SRC has an operating frequency range that extends both below and above the resonant frequency. This proves that the proposed SRC can provide a wider ZVS range than [27], since the operating frequency of the latter is only higher than the resonant frequency. Table 2 summarizes this comparison.

6. Conclusion

In this study, a three-phase series resonant tanks SRC with variable frequency control was proposed. This conceptualized converter contains certain attributes, as follows: (a) in comparison to the three-phase interleaved LLC resonant converter, the suggested converter might decrease how many power switches. are needed. This would have a major influence,

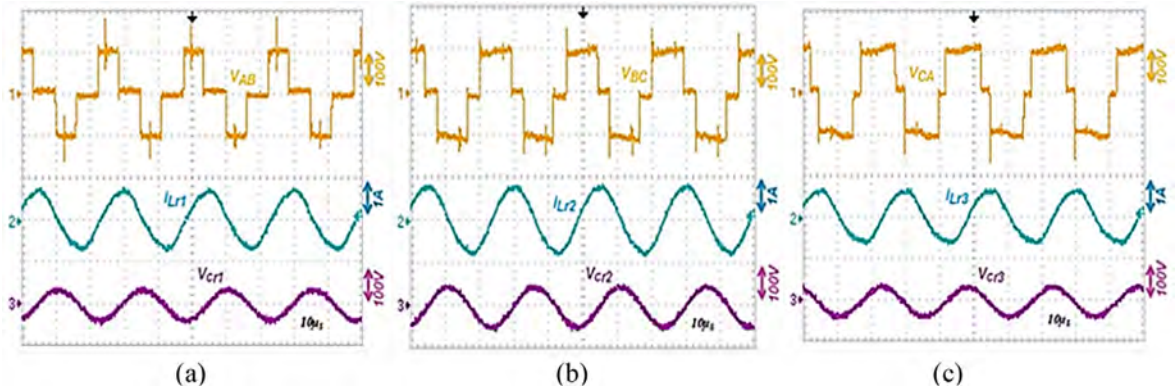

Fig. 13 Measured waveforms resonant tank voltage and current at full load; (a) Resonant tank input voltage V_{AB}, resonant inductor current i_{Lr1}, and resonant capacitor voltage v_{Cr1}. (b) Resonant tank input voltage V_{BC}, resonant inductor current i_{Lr2}, and resonant capacitor voltage v_{Cr2}. (c) Resonant tank input voltage V_{CA} resonant inductor current i_{Lr3}, resonant capacitor voltage v_{Cr3}.

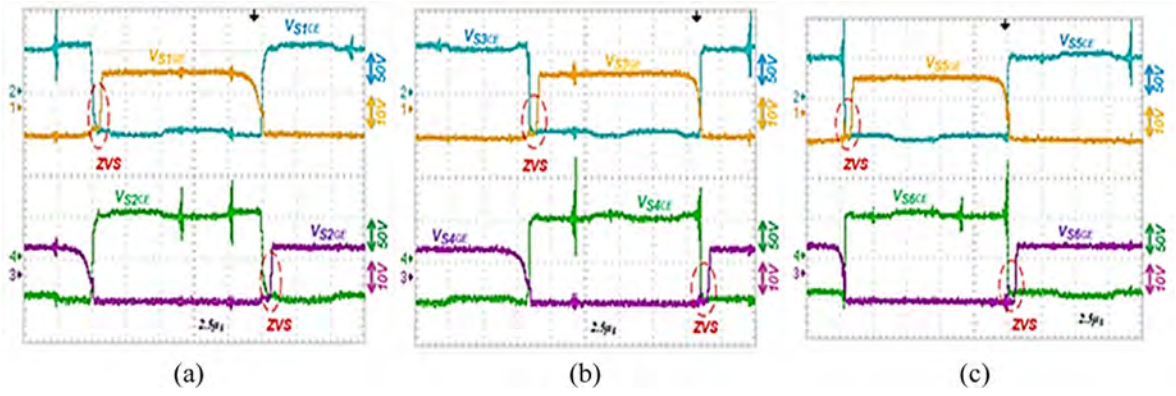

Fig. 14 Measured waveforms (MW) of the gate voltage V_{GE} and collector voltage V_{CE} for all the switches at 25% load; (a) S_1, and S_2, (b) S_3, and S_4, (C) S_5, and S_6.

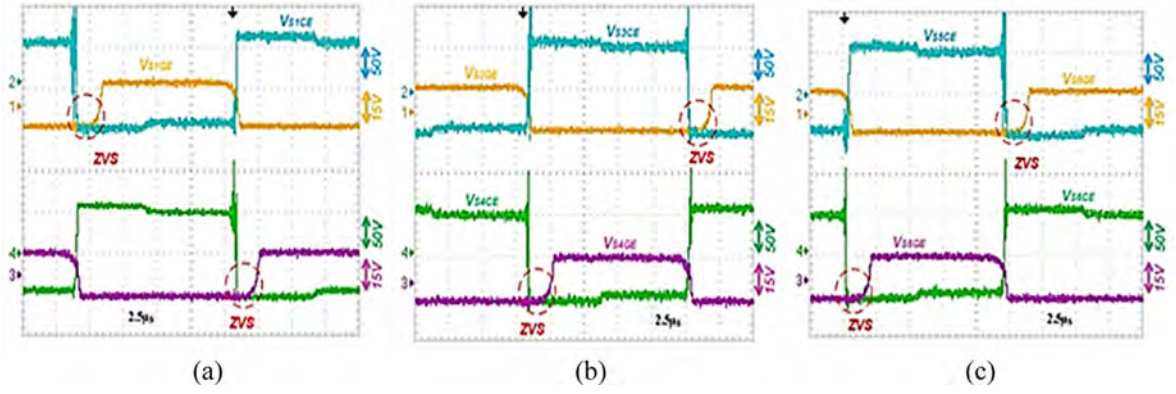

Fig. 15 Gate voltage V_{GE} and collector voltage V_{CE} for all the switches at 100% load; (a) S_1, and S_2, (b) S_3, and S_4, (C) S_5, and.S_6.

enabling weight reduction, lower cost, and a simpler circuit. (b) The utilized transformers' magnetizing inductance provide a broad ZVS range, within which the ZVS for the entire operating range of frequency and for every switch could be achieved by the suggested converter. (c) The suggested converter's output voltage is a six-fold increase over the input voltage. This indicates the suitability of the suggested converter for applications of high voltage. (d) With the suggested converter, variable switching frequency control was utilized and a wide load variation was maintained. This give confirmation that the load factor does not strictly affect any gain, since there is heavy reliance on the ratio of switching to resonant frequency.

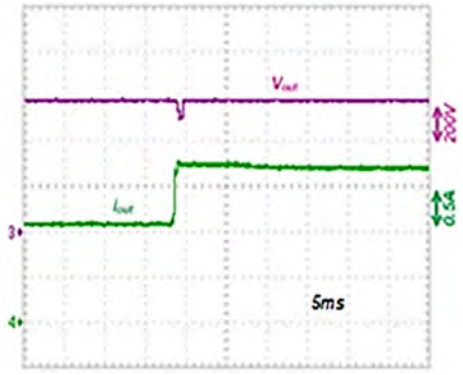

Fig. 16 Output voltage and current when the load is changed from $0.63kW$ to $1kW$.

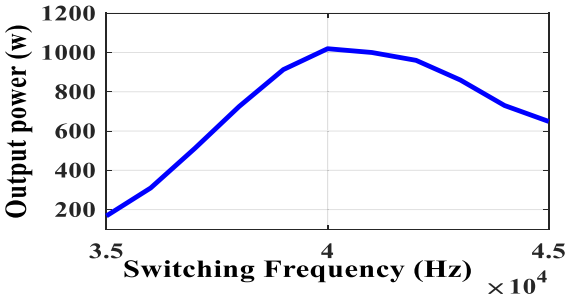

Fig. 17 Measured output power with different switching frequencies.

Furthermore, experimental findings from the laboratory demonstrate the performance of the system. The effectiveness of the theory-based have also been verified.

Declaration of Competing Interest

The authors declare that they have no known competing financial interests or personal relationships that could have appeared to influence the work reported in this paper.

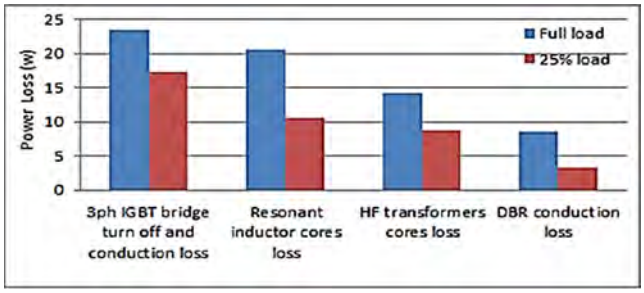

Fig. 19 Loss breakdown at full-load and 25% load, and $V_{in} = 100V$.

Acknowledgments

The authors would like to express their gratitude to Universiti Sains Malaysia, and the Research Creativity and Management Office (RCMO) for supporting and funding this research under Short-term grant No. 304/PELECT/6315330.

Appendix A. The detailed loss calculation methods for resonant converters have been studied in many literatures [34–37]. This appendix provides the loss expressions that are used to calculate the losses breakdown of the proposed converter. This loss model includes transistor (IGBT) losses, inductor core losses, transformer core losses, and the bridge rectifier diode losses. The equations used to calculate the losses are summarized briefly as below:

For primary three-phase IGBT's, since the switches are ZVS turned on, the turn-on losses of the inverter are negligible. Therefore, the turn off and the conduction losses of each IGBT are taken into account, which are

$$P_{IGBT\_cond} = R_{CE(on)} {I_{rms}}^2. \tag{A1}$$

While the turn-off losses of each IGBT by assuming that the current through its channel decreases linearly during IGBT turns off. The remaining current (which increases linearly) flows into its output capacitance C_{oes}, causing quadratic rise in the IGBT's V_{CE}[37]. The overlap between the channel current and the V_{CE} leads in losses, which can be expressed by:

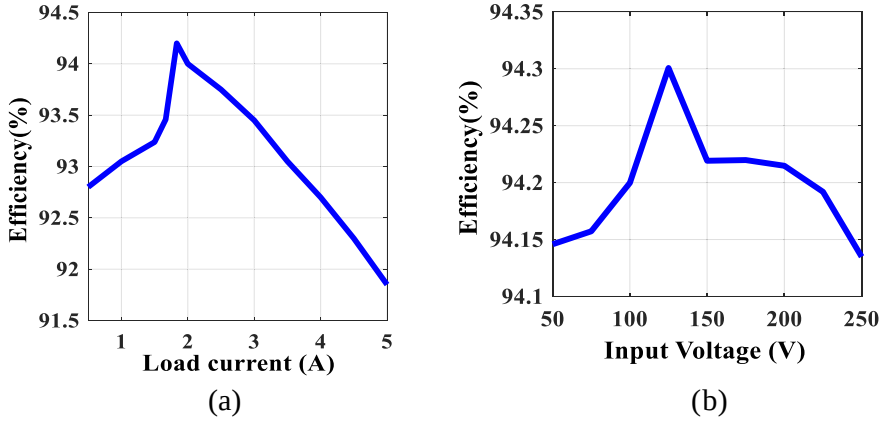

Fig. 18 Efficiency. (a) Different load currents with $V_{in} = 100V$. (b) Different input voltages at full load.

Table 2 Comparison of the proposed SRC converter with various existing converters.

Reference	Topologies	Number of the components	Input DC voltage, V	Output DC voltage, V	Switching frequency, kHz	Efficiency %
This work	Three-phase DC/DC Boost SRC with Variable Frequency Control.	Six power switches One transformer Three LC tanks	100–325	600	35–45	94.2%
[27]	"Three-phase three-level LC-type RC with variable frequency control"	Three LC tanks	440–590	400	53.34–80.42	94.5%
[28]	"Three-phase three-level DC/DC converter for high input voltage-adopting symmetrical duty cycle control"	Three transformers	540–600	48	50	85.5%
[33]	"Three-phase interleaved LLC RC employing the Y-connected rectifier"	Twelve power switches Three transformers Three LC tanks	380	300	34–39	95.5%

Table A1 Parameters for loss calculation.

$R_{CE(on)}$ $(m\Omega)$	t_{off} (ns)	C_{oes} (pf)	N_L	A_C (mm^2)	V_e (mm^3)	β	K_{fe} (w/cm^3T^{β})
84	110	265	64	76	5350	2.7	68

$$P_{IGBT\_off} = \frac{I_{off}{}^2 t^2{}_{off}}{48 C_{oes}} f_s. \quad \text{(A2)}$$

where $R_{CE(on)}$ is the on-state resistance of the IGBT, I_{rms} is the resonant current value which can be driven by using first harmonic approximation (FHA) as [35,38], t_{off} is the is the IGBT turn-off time, I_{off} is the current through the IGBT at the turn-off instant, and f_s is the switching frequency.

The power core loss of the resonant inductor $L_r$is derived as a function of resonant current as [35,38]

$$P_{Lr\_core} = K_{fe}\left(\frac{L_r}{N A_C}\right)^{\beta} V_e I_{Lr}{}^{\beta}. \quad \text{(A3)}$$

where K_{fe} and β represent properties of the used core material, $V_e$and A_C are the volume and the core cross-section area respectively, and N is the number of winding turns in inductor or transformer as they are listed in Table A1. This can be applied for the transformer with taking into account the number of used inductors and transformers.

The conduction loss of each diode in the diode bridge rectifier is

$$P_{Dr\_cond} = V_{Df} I_{avg} + I_{rms}{}^2 R_T. \quad \text{(A4)}$$

where $V_{Df}$is the forward voltage of each diode, I_{avg} is the average current through the diode, R_T is its on-state resistance, and I_{rms} is the RMS rectifier current value.

References

[1] H. Wang, Y. Chen, Y.-F. Liu, J. Afsharian, Z. Yang, A passive current sharing method with common inductor multi-phase LLC resonant converter, IEEE Trans. Power Electron. 32 (9) (2016) 6994–7010.

[2] H. Wu, Y. Lu, T. Mu, Y. Xing, A family of soft-switching DC–DC converters based on a phase-shift-controlled active boost rectifier, IEEE Trans. Power Electron. 30 (2) (2015) 657–667.

[3] B.-R. Lin, W.-J. Lin, Half-bridge zero voltage switching converter with three resonant tanks, J. Power Electron. 14 (5) (2014) 882–889.

[4] C.-H. Chien, Y.-H. Wang, B.-R. Lin, Analysis of a novel resonant converter with series connected transformers, IET Power Electron. 6 (3) (2013) 611–623.

[5] M.T. Outeiro, G. Buja, Comparison of resonant power converters with two, three, and four energy storage elements, in: Industrial Electronics Society, IECON 2015-41st Annual Conference of the IEEE, IEEE, 2015, pp. 001406–001411.

[6] C. Du, W.G. Hurley, D. Xu, Design methodology of resonant inductor in a ZVS inverter, IEEE J. Emerg. Select. Topics Power Electron. 3 (4) (2015) 1142–1150.

[7] M. Salem et al, Three-phase series resonant DC-DC boost converter with double LLC resonant tanks and variable frequency control, IEEE Access 8 (2020) 22386–22399.

[8] J. Jacobs, A. Averberg, R.D. Doncker, A novel three-phase DC/DC converter for high-power applications, in: 2004 IEEE 35th Annual Power Electronics Specialists Conference (IEEE Cat. No.04CH37551), vol. 3, 2004, pp. 1861–1867.

[9] G. Chen, X. Li, S. Zhou, Unified boundary control with phase shift compensation for dual bridge series resonant DC-DC converter, IEEE Access 8 (2020) 131137–131149.

[10] C.-H. Chien, Y.-H. Wang, B.-R. Lin, Series Resonant Converter with Series-Parallel transformers for high input voltage applications, in: TENCON 2011-2011 IEEE Region 10 Conference, IEEE, 2011, pp. 873–877.
[11] X. Xie, J. Zhang, C. Zhao, Z. Zhao, Z. Qian, Analysis and optimization of LLC resonant converter with a novel over-current protection circuit, IEEE Trans. Power Electron. 22 (2) (2007) 435–443.
[12] M.T. Outeiro, G. Buja, D. Czarkowski, Resonant power converters: an overview with multiple elements in the resonant tank network, IEEE Ind. Electron. Mag. 10 (2) (2016) 21–45.
[13] M. Salem, V.K. Ramachandaramurthy, P. Sanjeevikumar, Z. Leonowicz, V. Yaramasu, Full bridge LLC resonant three-phase interleaved multi converter for HV applications, in: 2019 IEEE international conference on environment and electrical engineering and 2019 IEEE industrial and commercial power systems Europe (EEEIC/I&CPS Europe), IEEE, 2019, pp. 1–6.
[14] B.-R. Lin, S.-F. Wu, ZVS resonant converter with series-connected transformers, IEEE Trans. Ind. Electron. 58 (8) (2011) 3547–3554.
[15] Y. Wei, Q. Luo, D. Woldegiorgis, H. Mhiesan, A. Mantooth, Characteristics analysis of LLC and LCL-T resonant tank, In: 2020 IEEE Transportation Electrification Conference & Expo (ITEC), Chicago, IL, USA, 2020, pp. 427–432.
[16] M. Salem, A. Jusoh, N.R.N. Idris, H.S. Das, I. Alhamrouni, Resonant power converters with respect to passive storage (LC) elements and control techniques – an overview, Renew. Sustain. Energy Rev. 91 (2018) 504–520.
[17] K. Jin, X. Ruan, Hybrid full-bridge three-level LLC resonant ConverterA novel DC DC converter suitable for fuel-cell power system, in: IEEE Transactions on Industrial Electronics, vol. 53, no. 5, 2006, pp. 1492–1503.
[18] C.-H. Chang, C.-A. Cheng, H.-L. Cheng, Modeling and design of the llc resonant converter used as a solar-array simulator, IEEE J. Emerg. Select. Topics Power Electron. 2 (4) (2014) 833–841.
[19] G. Ivensky, S. Bronshtein, A. Abramovitz, Approximate analysis of resonant LLC DC-DC converter, IEEE Trans. Power Electron. 26 (11) (2011) 3274–3284.
[20] M.K. Kazimierczuk, D. Czarkowski, Resonant Power Converters, John Wiley & Sons, 2012.
[21] Y. Ren, M. Xu, J. Sun, F.C. Lee, A family of high power density unregulated bus converters, IEEE Trans. Power Electron. 20 (5) (2005) 1045–1054.
[22] S. M. Tayebi, W. Xu, H. Wang, R. Yu, Z. Guo, A.Q. Huang, A single-stage isolated resonant SiCDC/AC inverter for efficient high-power applications, in: 2020 IEEE Applied Power Electronics Conference and Exposition (APEC), New Orleans, LA, USA, 2020, 399–404.
[23] I.O. Lee, G.W. Moon, Three-level LLC SRC for high and wide input voltage applications, in: 8th International Conference on Power Electronics – ECCE Asia, 2011, pp. 52–59.
[24] L. Colalongo, G. Duina, A. Richelli, Z.M. Kovacs-Vajna, A modular boost converter with low switch stress and high conversion ratio for automotive applications, in: 2018 International Conference of Electrical and Electronic Technologies for Automotive, IEEE, 2018, pp. 1–4.
[25] X. Wang, G. Tang, Z. He, X. Wei, H. Pang, X. Xiao, Modeling and control of an isolated module multilevel DC/DC converter for DC grid, CSEE J. Power Energy Syst. 3 (2) (2017) 150–159.
[26] J. Li, X. Zuo, Y. Zhao, X. Lv, J. Wang, Operation, analysis and experiments of DC transformers based on modular multilevel converters for HVDC applications, CSEE J. Power Energy Syst. 5 (1) (2019) 87–99.
[27] F. Liu, Y. Chen, X. Chen, Comprehensive analysis for three-phase three-level LC-type resonant DC/DC converter with variable frequency control-series resonant converter, IEEE Trans. Power Electron. 32 (7) (2017) 5122–5131.
[28] F. Liu, G. Hu, X. Ruan, Three-phase three-level dc/dc converter for high input voltage and high power applications-adopting symmetrical duty cycle control, IEEE Trans. Power Electron. 29 (1) (2014) 56–65.
[29] B.-R. Lin, S.-K. Chung, T.-Y. Shiau, Zero-voltage-switching DC/DC converter with three three-level pulse-width modulation circuit cells, IET Power Electron. 6 (1) (2013) 1–8.
[30] Y. Shi, X. Yang, Wide range soft switching PWM three-level DC–DC converters suitable for industrial applications, IEEE Trans. Power Electron. 29 (2) (2014) 603–616.
[31] S. Becchetti, A. Richelli, L. Colalongo, Z. Kovacs-Vajna, A comprehensive comparison of EMI immunity in CMOS amplifier topologies, Electronics 8 (10) (2019) 1181.
[32] J. Rabkowski, D. Peftitsis, H.-P. Nee, Parallel-operation of discrete SiC BJTs in a 6-kW/250-kHz DC/DC boost converter, IEEE Trans. Power Electron. 29 (5) (2014) 2482–2491.
[33] H.-S. Kim, J.-W. Baek, M.-H. Ryu, J.-H. Kim, J.-H. Jung, The high-efficiency isolated ac–dc converter using the three-phase interleaved LLC resonant converter employing the Y-connected rectifier, IEEE Trans. Power Electron. 29 (8) (2014) 4017–4028.
[34] Z. Guo, D. Sha, X. Liao, Hybrid phase-shift-controlled three-level and LLC DC–DC converter with active connection at the secondary side, IEEE Trans. Power Electron. 30 (6) (2015) 2985–2996.
[35] C. Chen, X. Zhao, J. Lai, A PWM controlled active boost quadrupler resonant converter for high step-up application, in: 2019 IEEE Applied Power Electronics Conference and Exposition (APEC), Anaheim, CA, USA, 2019, pp. 2317–2321.
[36] Y. Ang, C.M. Bingham, M.P. Foster, D.A. Stone, Modelling and regulation of dual-output LCLC resonant converters, in: IECON 2007–33rd Annual Conference of the IEEE Industrial Electronics Society, 2007, pp. 2130–2135.
[37] Y. Chen, H. Wang, Z. Hu, Y.F. Liu, J. Afsharian, Z.A. Yang, LCLC resonant converter for hold up mode operation, in: 2015 IEEE Energy Conversion Congress and Exposition (ECCE), 2015, pp. 556–562.
[38] S. Zong, H. Luo, W. Li, Y. Deng, X. He, Asymmetrical duty cycle-controlled LLC resonant converter with equivalent switching frequency doubler, IEEE Trans. Power Electron. 31 (7) (2016) 4963–4973.
[39] U. Kundu, K. Yenduri, P. Sensarma, Accurate ZVS analysis for magnetic design and efficiency improvement of full-bridge LLC resonant converter, IEEE Trans. Power Electron. 32 (3) (2017) 1703–1706.